Classical description of strong-field double ionization by elliptical laser pulses

Yueming Zhou,[1] Qingbin Zhang,[1,*] Cheng Huang,[1] and Peixiang Lu[1,2,*]

[1]*School of Physics, Huazhong University of Science and Technology, Wuhan 430074, People's Republic of China*

[2]*Key Laboratory of Fundamental Physical Quantities Measurement of Ministry of Education, China*

(Received 19 August 2012; published 24 October 2012)

Sequential double ionization of argon induced by elliptically polarized laser pulses at the over-the-barrier ionization regime is investigated with a fully classical model. We provide futher detail beyond that found in our previous paper [Phys. Rev. Lett. **109**, 053004 (2012)] and show that all of the experimental observations, including the evolution of the ion momentum spectra as a function of laser intensity, the intensity-dependent ratio for the parallel and antiparallel electron emissions, and the release times of both electrons for various laser pulses, are excellently reproduced by our classical model. Our results indicate that the classical treatment is very valid and accurate in describing strong-field ionization, providing a simple and intuitive way to investigate the complex electron correlations in strong-field double and multiple ionizations.

DOI: 10.1103/PhysRevA.86.043427 PACS number(s): 32.80.Rm, 31.90.+s, 32.80.Fb

I. INTRODUCTION

Strong-field double ionization (DI) has been extensively investigated during the past decades, both theoretically and experimentally. It has been found that two different types of physical mechanisms underlie this phenomenon: nonsequential double ionization (NSDI) and sequential double ionization (SDI). At the linearly polarized and moderate intensity laser field, DI is dominated by the nonsequential process, where the second electron is ionized by the recollision of the first electron [1]. Because of the recollision, the two electrons from NSDI exhibit a highly correlated behavior, which has attracted particular interest during the past years [2–20]. When the laser intensity is high enough, the second electron can be ionized by the laser field without the recollision of the first tunneled electron, and SDI becomes the dominant process [21–23]. The SDI process also dominates in the case of the circularly polarized field, where recollision is essentially forbidden [24,25]. In SDI, it is usually accepted that there is no correlation between the two involved electrons and the two ionization steps can be treated independently by the tunneling theory. Consequently, most of the previous studies are focused on NSDI, and there is a lack of studies on SDI. However, investigation into SDI can provide some information that has been covered in NSDI due to the recollision. For example, by measuring the electron momentum from SDI in the elliptically polarized pulses, one can obtain the release times of the electrons [26,27]. Recently, Pfeiffer *et al.* performed such an experiment to time the release of electrons in SDI [28]. It is found that the release time of the first electron agrees well with the prediction of standard independent-tunneling theory. However, the release time of the second electron is much earlier than prediction of independent-tunneling theory [28]. It is also presented that the ratio of the parallel to antiparallel emissions of the SDI events shows an oscillating behavior as a function of the laser intensity, which is in conflict with predictions of the standard independent-tunneling theory [29]. In Ref. [30], it has been shown that there is a clear angular correlation between the two electrons from SDI, which also implies that the successive ionization steps of SDI are not independent. These results imply that our understanding of SDI is far from being complete and that the electron correlations should be treated more delicately.

On the theoretical side, accurate description of SDI needs full quantum theory. However, it requires enormous computational demand to solve the fully dimensional time-dependent Schrödinger equation (TDSE) of the two-electron system. Currently, it has only been performed for NSDI by the linearly polarized laser fields [15]. It is a task of great challenge to extend this method to SDI, which occurs at much higher intensities or a circularly polarized laser field. Instead, in the past decades numerous approximative methods have been widely employed to investigate the multielectron processes in strong laser fields, e.g., numerical solution of the TDSE within the reduced dimensionality [17] and many-body *S*-matrix theory based on strong-field approximation [16]. Especially, classical models have been well established and have provided an intuitive insight into the electron dynamics within the recollision scenario [18–20]. However, the classical models are standing at the qualitative level in explaining the strong-field ionizations [18–20,31–33]. Can a classical method describe the strong-field ionization processes quantitatively? In our previous Letter, we demonstrated that a fully classical model is able to complete this mission [34]. There, as an example, we showed that the release times of the two electrons in SDI, which cannot be predicted by the standard independent-tunneling theory, are quantitatively reproduced by our classical model [34].

Following our previous Letter [34], in this paper we present more detail on our classical model and extend our calculations to demonstrate that all of the experimental observations are excellently reproduced by our classical calculations. For instance, our numerical results show that the momentum distribution of the doubly charged ion in the direction of the minor axis of laser polarization depends on the laser intensity; it exhibits a bifurcation structure from a three-peak structure at the relatively low laser intensities to a four-peak structure at the relatively high laser intensities, which is in excellent agreement with the experimental results. The corresponding processes for this bifurcation are presented intuitively by tracing the

*Corresponding author: zhangqingbin@gmail.com; lupeixiang@mail.hust.edu.cn

SDI trajectory. We show that the experimentally measured ionization times of the two electrons for various pulse durations are well reproduced by our classical calculations. These results indicate that the classical method is valid and very accurate in describing the strong-field SDI. Consequently, our work provides a simple and reliable way to investigate multielectron dynamics in SDI.

This paper is organized as follows. In Sec. II we describe our classical model. Then we display our results and discussions in Sec. III. Finally, we summarize our paper in Sec. IV.

II. THE HEISENBERG-CORE POTENTIAL CLASSICAL MODEL

In a classical model of the two-electron system, one electron often drops deeply into the Coulomb potential well, leading to autoionization of the other electron. Thus, the problem in the classical model of the two-electron system that has to be solved is to avoid autoionization. This problem can be solved by employing the soft-core potential instead of the Coulomb potential for the ion-electron interaction. In the past decade, the soft-core potential classical model (SPCM) has achieved great success in exploring the correlated electron dynamics in NSDI [19,20,31]. The disadvantage of the SPCM is that it cannot match the first and the second ionization potentials of the model atom with the realistic atom. In fact, the first electron often ionizes, leaving the second electron at a state with an energy much lower than the second ionization potential of the investigated target [35]. This disadvantage is not a serious problem in NSDI because the crucial step for NSDI is recollision, which is insensitive to the second ionization potential. However, for SDI, both the first and the second electrons are ionized through tunneling or over the barrier. Thus the ionization rate of both electrons depends exponentially on the ionization potential. Consequently, in order to describe SDI accurately, it is necessary to make ionization potentials of the first and the second electrons match with the realistic target. In our previous Letter [34], we employed the Heisenberg-core potential instead of the soft-core potential in the classical two-electron model to study SDI, and a surprisingly high accuracy was achieved. The Heisenberg-core potential was originally introduced by Kirschbaum and Wilets [36] and it was later developed and widely used in atomic and molecular collisions [37,38] and strong-field ionization [39]. In these studies, the Heisenberg-core potential was introduced to account for the Heisenberg uncertainty principle, which makes the multielectron system stable. It has been shown that the Heisenberg-core potential not only prevents autoionization but also gives the energy-configuration of the multielectron systems [34,36–38].

The Heisenberg-core potential is written as

$$V_H(r_i,p_i)=\frac{\xi^2}{4\alpha r_i^2}\exp\left\{\alpha\left[1-\left(\frac{r_i\,p_i}{\xi}\right)^4\right]\right\}, \qquad (1)$$

where the parameter α indicates the rigidity of the Heisenberg core. For a given α, the parameter ξ is chosen to match the second ionization potential of the target. r_i and p_i are the position and canonical momentum of the ith electron, respectively. The Hamiltonian of the two-electron atom in the Heisenberg-core potential classical model is (atomic units are used throughout this paper unless stated otherwise)

$$H_1=\frac{1}{|\mathbf{r}_1-\mathbf{r}_2|}+\sum_{i=1,2}\left[-\frac{2}{r_i}+\frac{\mathbf{p}_i^2}{2}+V_H(r_i,p_i)\right]. \qquad (2)$$

In our calculations, the rigidity parameter α is set to be 2. When α is set, the parameter ξ is chosen to make the minimum of the one-electron Hamiltonian equal to the second ionization potential of the investigated target [34]. For Ar, we obtain $\xi=1.259$. The ground-state energy of the two-electron model atom is set by summing the first and the second ionization potentials of Ar (-1.59 a.u.). Regretfully, for the values of parameters $\alpha=2$ and $\xi=1.259$, we could not place the two electrons in the classically allowed phase space with the energy of -1.59 a.u. Thus, we chose $\alpha=2$ and $\xi=1.225$. For these values, the corresponding second ionization potential of the model atom is -1.065 a.u., deviating a little from the realistic target (-1.02 a.u.). This small deviation does not influence our results. In this paper, we choose $\alpha=2$ and $\xi=1.225$ unless we discuss the parameter dependence. It should be mentioned that in our classical model, the potential of the ion-electron interaction is different from the Coulombic potential because of the Heisenberg potential. But the Heisenberg-core potential vanishes quickly as the distance increases. For tunneling and over-the-barrier ionization the exit point is often several atomic units away from the core where the Heisenberg-core potential almost disappears and thus the ion-electron potential is almost recovered to the Columbic potential.

The initial state of the classical ensemble is obtained as follows: First, the electrons were located at the opposite sides of the nucleus, and the available kinetic energy was distributed between the two electrons randomly in phase space. Then, the system was allowed to evolve at the absence of the laser field. After a sufficient long time, the ensemble reached a stable distribution in phase space, which is shown in Fig. 1. As shown in Figs. 1(a) and 1(b), the electrons are prevented from visiting the vicinity of the nucleus, which results from the Heisenberg-core potential. The characteristic makes the two-electron model atom free from autoionization. Though this distribution is somewhat different from that of the realistic atom, it still works because the part of electric distribution for ionization is from the outer regime.

When the initial state is obtained, the evolution of the system is determined by the equations

$$\frac{d\mathbf{r}_i}{dt}=\frac{\partial H}{\partial \mathbf{p}_i},\quad \frac{d\mathbf{p}_i}{dt}=-\frac{\partial H}{\partial \mathbf{r}_i}, \qquad (3)$$

where H is the Hamiltonian of the two-electron system in the presence of the laser field, i.e., $H=H_0+(\mathbf{r}_1+\mathbf{r}_2)\cdot\mathbf{E}(t)$. $\mathbf{E}(t)$ is the electric field of the laser pulses. In our calculations it is set to be the same as that in the experiment, i.e., it is written as $\mathbf{E}(t)=f(t)[\frac{\varepsilon}{\sqrt{\varepsilon^2+1}}\cos(\omega t+\varphi)\hat{\mathbf{x}}+\frac{1}{\sqrt{\varepsilon^2+1}}\sin(\omega t+\varphi)\hat{\mathbf{y}}]$, where $f(t)=E_0\exp[-\frac{1}{2}(\frac{2\sqrt{\ln 2}t}{\tau})^2]$ is the field envelope; ω, ε, and φ are the laser frequency, the ellipticity, and the carrier-envelope phase (CEP), respectively; and τ denotes the pulse duration (FWHM). In our calculations, we employed two pulses, one with a duration of 7 fs and the other with a duration of 33 fs. The wavelength and ellipticity for the 7-fs (33-fs) pulse are, respectively, 740 nm (788 nm) and 0.78 (0.77), same as those in the experiment [28].

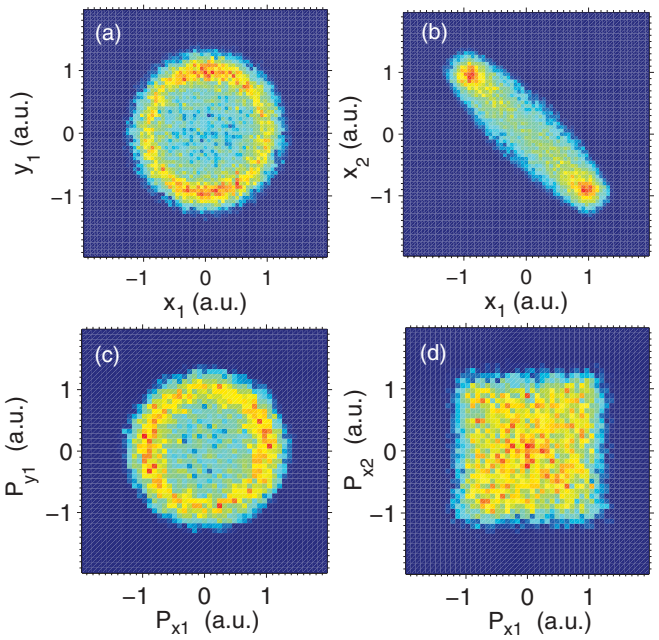

FIG. 1. (Color online) The initial distributions of the electrons in phase space. The energy of the two-electron system is set to be −1.59 a.u., i.e., the sum of the first and the second ionization potentials of Ar. Here (x_i, y_i, z_i) and (P_{xi}, P_{yi}, P_{zi}) represent the coordinates and the momenta of the ith electron in the directions of the $\hat{x}$, $\hat{y}$, and $\hat{z}$ axes, respectively.

In order to compare our numerical results with experiment, the volume effect has been considered in our calculations. For a peak intensity I_0, the signal $S(I_0)$ is obtained by integrating the intensity-dependent signal over a three-dimensional Gaussian beam:

$$S(I_0) = \int_0^{I_0} S(I)\left[-\frac{\partial V(I_0, I)}{\partial I}\right] dI. \tag{4}$$

Here $S(I)$ is the signal at intensity I, $[-\frac{\partial V(I_0,I)}{\partial I}]dI$ is the volume inside the isointensity shell dI at I, and $V(I_0,I)$ is the volume between the intensity I and I_0. For the three-dimensional Gaussian beam, $V(I_0,I)$ is given by [40] $V(I_0,I) = \pi\omega_0^2 z_R[\frac{4}{3}\beta^{1/2} + \frac{2}{9}\beta^{3/2} - \frac{4}{3}\arctan\beta^{1/2}]$, where $\beta = [(I_0/I) - 1]$, ω_0 is the beam radius at the focus, and z_R is the Rayleigh range. In practice, the integration of Eq. (4) is running from 0.5 PW/cm^2 to I_0 because the SDI yield at intensities below 0.5 PW/cm^2 is very low.

We remark that in our classical model, we only considered two active electrons while we ignored the inner shell of the atom. Our model is a simple model for SDI. The multielectron effect from the inner electrons is not contained, and the effect on DI is not clear at present. Almost all of the previous studies on strong-field DI are based on this treatment, and the feats of the two-active-electron models are remarkable [15–20]. In our classical model, there is no tunneling ionization and all of the electrons are ionized by over-the-barrier escape. In this paper, the main calculations are performed at intensities higher than 1.0 PW/cm^2, where the tunneling ionization is negligible. Thus the classical treatment is valid. Because of the high laser intensity, the contribution from the quantum excited state can also neglected because an electron in the excited state can be quickly ionized by the laser field.

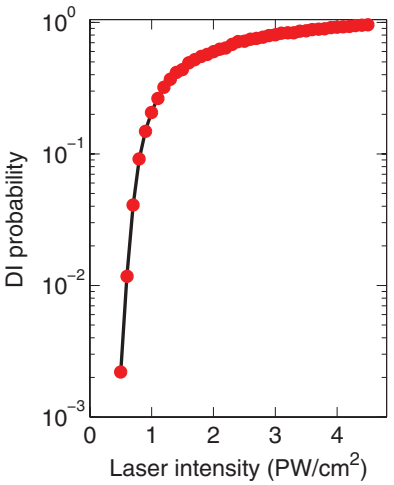

FIG. 2. (Color online) The DI yield as a function of laser intensity. The pulse duration is 33 fs and the ellipticity is 0.77.

III. RESULTS AND DISCUSSIONS

First of all, in Fig. 2 we show the DI yield as a function of the laser intensity calculated by our classical model. It is clearly seen that at intensities below 1.0 PW/cm^2, the DI yield increases rapidly as the laser intensity increases. When the laser intensity further increases, the DI yield rises slowly and approaches the saturation gradually. In the present paper, we focus our calculations in the intensity regime near and at the saturate intensity.

Figure 3 displays the electron [(a) and (b)] and the ion [(c) and (d)] momentum distributions in the laser polarization plane. The laser duration is 7 fs and the laser intensities are 2.0 PW/cm^2 (left column) and 4.0 PW/cm^2 (right column), respectively. Here the volume effect was not considered. In Figs. 3(a) and 3(b) we show the momentum distributions of one electron, without distinguishing whether it is the first or the second electron. It is clearly shown that the population is more likely to be clustered around the x axis. This is due to the fact that the extremes of the electric field in the y direction are stronger than those in the x direction, and thus the electrons prefer emission along the y axis. The electron that emits along the y axis at the times of y maximum of the electric field achieves a final momentum with a large x component [32]. It is shown in Figs. 3(a) and 3(b) that the distributions exhibit two maxima at the relatively low laser intensity and four maxima at the relatively high laser intensity. This phenomenon can be explained as follows: At the high laser intensity, the first electron is depleted before the peak of the pulse. Thus, the release time of the first electron is much earlier than that of the second electron. Consequently, the amplitude of the final momentum of the second electron is larger than that of the first electron. The two inner maxima in Fig. 3(b) correspond to the first electron and the two outer maxima correspond to the second electron [28]. At the relatively low laser intensity, both electrons are ionized around the peak of the laser pulse. Thus, the amplitudes of

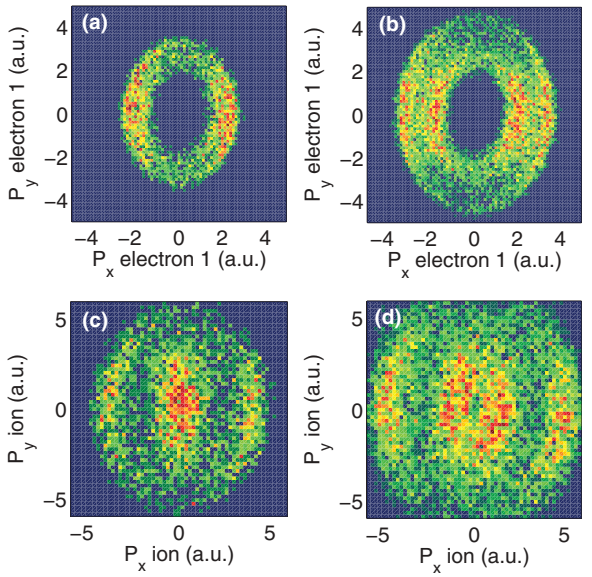

FIG. 3. (Color online) (a) and (b) Momentum distributions for one of the two electrons from SDI in the laser polarization plane. (c) and (d) Momentum distributions of the doubly charged ion in the laser polarization plane. The pulse duration is 7 fs. The laser intensities are (a) and (c) 2.0 PW/cm^2, and (b) and (d) 4.0 PW/cm^2. The CEP is randomly chosen for each trajectory.

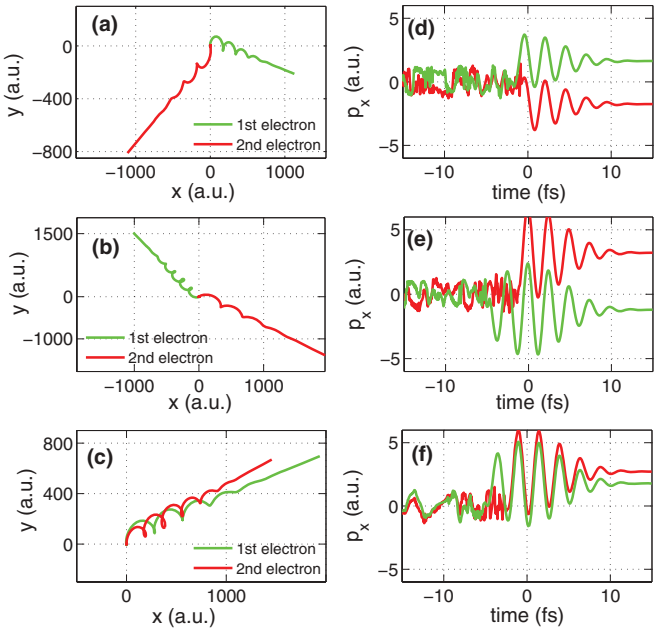

FIG. 4. (Color online) (a)–(c) Three illustrative trajectories in the laser polarization plane. (d)–(f) Time evolution of electron momenta in the direction of the minor axis for the trajectories shown in (a)–(c), respectively.

the final momenta for the first and the second electrons are almost the same. Consequently, the two left maxima (the two with negative momenta) and the two right maxima (the two with positive momenta) are, respectively, evolving into one maximum [28], as shown in Fig. 3(a). The above analysis also explains the ion momentum distributions shown in Figs. 3(c) and 3(d). At the relatively high laser intensity, the distribution exhibits a four-band structure. The outer and the inner two bands correspond to the events where the two electrons emit into the same and opposite hemispheres, respectively. At the relatively low laser intensity, the antiparallel emissions result in the nearly zero momentum of the ion. Thus the two inner bands join together, locating at zero momentum.

To address the processes stated above intuitively, in Fig. 4 we display three illustrative trajectories. The left column shows the coordinates of trajectories of electron pairs in the polarization plane. The right column displays the corresponding time evolution of the electron momenta in the direction of the minor elliptical axis. For the trajectory shown in Fig. 4(a), the two electrons emit into the opposite hemispheres. Because both electrons emit near the peak of the laser pulse, the final momenta of the two electrons have similar amplitudes but opposite directions, as shown in Fig. 4(d). This kind of trajectory results in the middle band shown in Fig. 3(c). For the trajectory shown in Fig. 4(b), the two electrons also emit into the opposite hemispheres. However, the first electron (the green [light] curve) escapes much earlier than the second electron (the red [dark] curve). Thus the final momenta of the two electrons have opposite directions and very different amplitudes [see Fig. 4(e)]. This kind of trajectory is responsible for the inner two bands in the ion momentum distribution of Fig. 3(d). For the trajectory shown in Fig. 4(c), the two electrons emit into the same hemisphere and they achieve final momenta with the same direction, as displayed in Fig. 4(f). This trajectory accounts for the two outer bands of the ion momentum spectra shown in Figs. 3(c) and 3(d).

In the following, we give more detailed comparison of our numerical results with the experimental data [28]. First, we show the ratio of the parallel and antiparallel emissions along the minor elliptical axis in Fig. 5. In the experiment, it has been shown that in SDI the ratio of the parallel and antiparallel emissions exhibits an oscillating behavior as a function of laser intensity [28]. This oscillating behavior has been explained as a result of the multielectron effect [33]. In our calculations, this oscillation is nicely reproduced, as shown in Fig. 5. In the experiment, it is also found that the oscillating curve is a bit below 1. Without theoretical investigation, this behavior might be ascribed to the different detection efficiencies for the parallel and antiparallel events. In our numerical results,

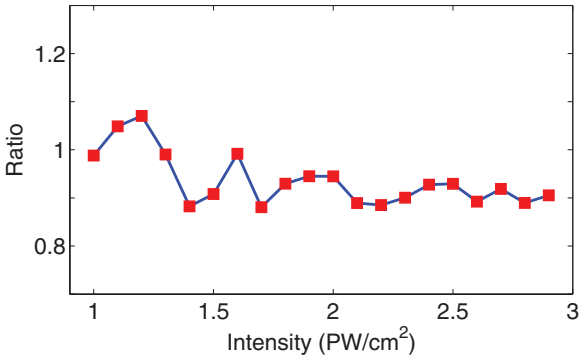

FIG. 5. (Color online) The ratio of the SDI counts of parallel and antiparallel emissions along the minor elliptical axis, as a function of the laser intensity. The pulse duration is 7 fs. The CEP is randomly chosen for each trajectory.

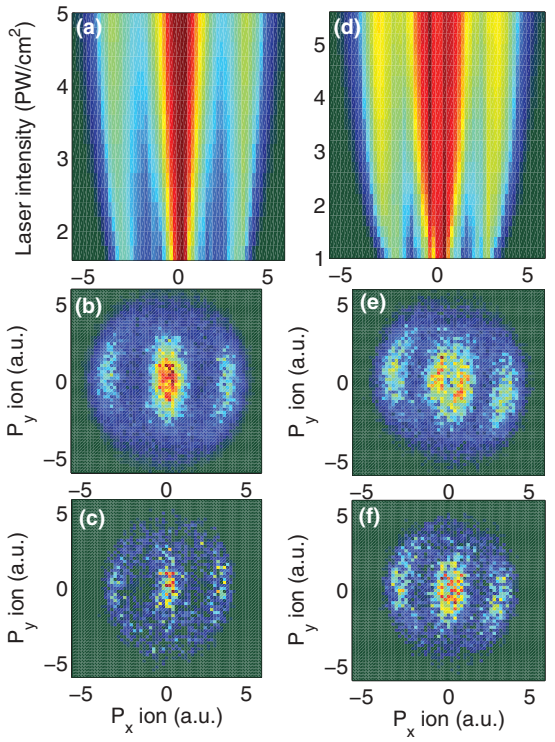

FIG. 6. (Color online) (a) Ion momentum distribution along the direction of the minor elliptical axis, as a function of laser intensity. (b) Ion momentum distribution in the laser polarization plane. The laser intensity is 3.5 PW/cm^2. (c) The same as (b) but the laser intensity is 1.5 PW/cm^2. The pulse duration for (a)–(c) is 7 fs. The CEP is randomly chosen for each trajectory. (d)–(f) The same as (a)–(c) but for the 33-fs pulses. In these calculations the volume effect has been considered.

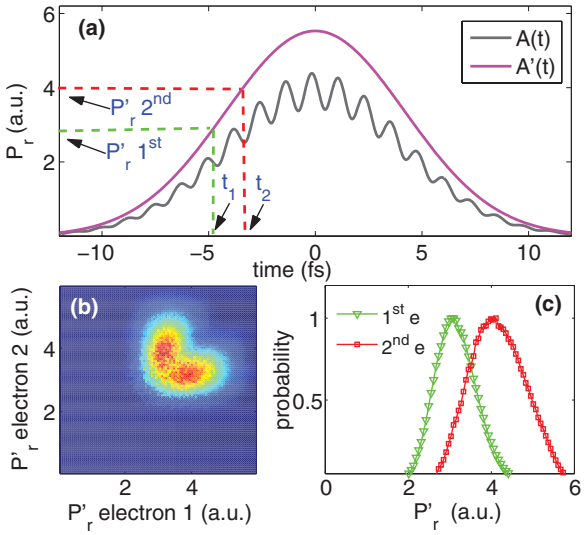

FIG. 7. (Color online) Sketch of the time-reading procedure. (a) The grey (lower) curve shows the vector potential $A(t)$, where $A(t) = \sqrt{A_x(t)^2 + A_y(t)^2}$. The magenta (upper) curve denotes the scaled vector potential $A'(t)$, where $A'(t) = \sqrt{[(\epsilon^2+1)/\epsilon^2]A_x(t)^2 + (\epsilon^2+1)A_y(t)^2}$. (b) The electron correlation spectrum for the scaled radial momentum p'_r. (c) We display the scaled radial momentum spectra of the first and the second electrons separately.

the oscillating curve is also below 1. Thus, it convincingly confirms that this behavior is not due to the different detection efficiencies. The two electrons are indeed more likely to emit into the opposite hemispheres.

In Ref. [28] it has been shown that the ion momentum distribution along the minor elliptical axis exhibits a characteristic dependence on laser intensity: For the 33-fs pulses, there is a bifurcation from a three-peak structure to a four-peak structure as the laser intensity increases. In Fig. 6, we present our numerical results. The left and the right columns show the ion momentum distribution for the 7-fs and 33-fs pulses, respectively. Here, the volume effect has been taken into account. It is clearly shown that for the 33-fs pulses the distribution exhibits a three-peak structure at the low laser intensities and gradually evolves into a four-peak structure as the laser intensity increases. The bifurcation appears at an intensity of about 2.5 PW/cm^2, consistent with experimental results [28]. In Figs. 6(e) and 6(f) we display the ion momentum distribution in the polarization plane at intensities of 3.5 and 1.5 PW/cm^2, respectively. The four-peak structure at the high laser intensity and the three-peak structure at the low laser intensity are more clearly seen. For the 7-fs pulses, it has been shown in previous experimental papers [26,29] that the ion distribution exhibits a three-peak structure even at the high laser intensity region. Figure 6(a) shows our numerical results for the 7-fs pulses. The distribution exhibits a three-peak structure even in the very high laser intensity region, also consistent with experimental results.

It has been demonstrated that the elliptical laser pulses could act as a clock to measure the electron release time in strong-field ionization [26]. In Ref. [28], the release times of the two electrons in SDI were measured. It is found that the release time of the first electrons can be well predicted by the standard independent-tunneling theory. However, it is a great surprise that the second electron is ionized much earlier than the prediction of the independent-tunneling theory. Here we show the release times of the two electrons calculated by our classical model and compare them with the experimental data. First, in Fig. 7 we show the procedure of determining the release times in the experiment and our calculations. In general, the electron momentum of the elliptical laser field is not an injective function of time, but a new scaled radial momentum p'_r is an injective function with the condition that the electron is ionized before the peak of the pulses [28]. The scaled radial momentum p'_r is obtained as

$$p'_{1r} = \sqrt{[(\epsilon^2+1)/\epsilon^2]p_{1x}^2 + (\epsilon^2+1)p_{1y}^2}, \quad (5)$$

$$p'_{2r} = \sqrt{[(\epsilon^2+1)/\epsilon^2]p_{2x}^2 + (\epsilon^2+1)p_{2y}^2}. \quad (6)$$

Figure 7(b) displays the correlated spectrum of p'_{1r} and p'_{2r}. This spectrum is symmetric with respect to the diagonal because we do not distinguish which one is the first and which one is the second electron. The repulsion behavior along the diagonal means the different final momentum of the two electrons and thus indicates their different release times. In Fig. 7(c) we distinguish the two electrons with the assumption

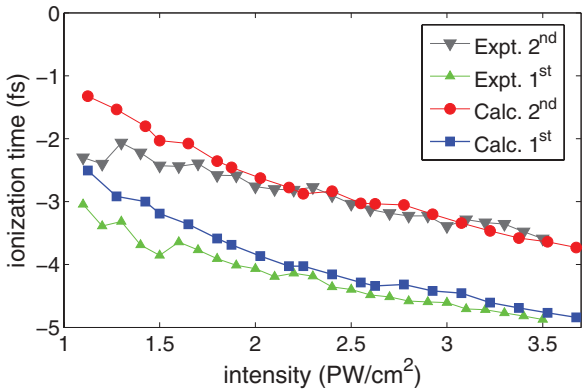

FIG. 8. (Color online) The release times of the first and the second electrons in SDI by the 7-fs pulses. The experimental data from Ref. [28] are also shown for comparison. The volume effect has been considered.

that the first electron carries a smaller radial momentum. Then the release time of the electron is determined by projecting the peak position of the corresponding spectrum of Fig. 7(c) to the scaled vector potential, as sketched in Fig. 7(a).

In Fig. 8 we show the release times of the two electrons in the 7-fs pulses. For comparison, the experimental data from Ref. [28] is also shown. Note that for our numerical results the laser intensity in Fig. 8 has been scaled with a constant factor of 0.8, which is well within the experimental uncertainty. It is a great surprise that the numerical results from a simple classical model agree so well with the experimental results. The results for the 33-fs pulses are shown in Fig. 9. Obviously, the numerical results also agree with the experimental data quantitatively. Hereto, we have shown that our fully classical model excellently reproduced all of the experimental observations. During the past decades classical models have achieved great success in exploring the strong-field ionization process. But all of them were standing at the qualitative level. Our work has demonstrated that a classical treatment is capable of describing the strong-field processes at the quantitative level.

In Ref. [28], the authors neglected the initial velocity at ionization and the Coulomb interaction between the ion and the escaping electron when calculating the ionization times

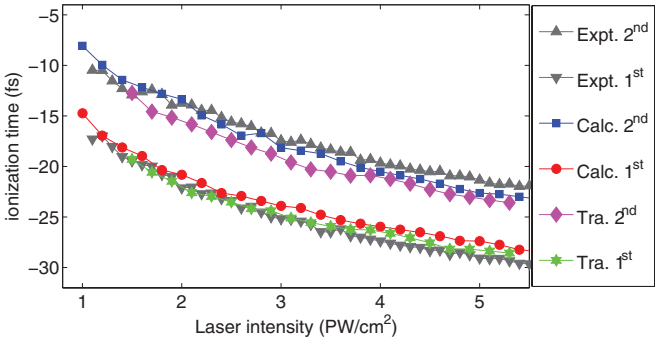

FIG. 9. (Color online) The release times of the first and the second electrons in SDI by the 33-fs pulses. The experimental data from Ref. [28] are also shown for comparison. We also show the release times of two electrons obtained by tracing the classical trajectories (see text for details). The volume effect has been considered.

with the tunneling theory. A question remains: Does the deviation of the second ionization time between the experiment and prediction of the tunneling theory result from these approximations? Our classical method enables us to answer this question by tracing the classical trajectories. In order to do this, first we extract the release times of the electrons at each intensity of focal volume by tracing the classical trajectories. Next we obtain the final momenta with the formula $\int_{t_i}^{+\infty} -\mathbf{E}(t)dt$, where t_i is the traced release time and $\mathbf{E}$ is the electric field. In this formula, we neglect the initial momentum and the Coulomb interaction between the ion and the escaping electron, same as that in the tunneling theory of Ref. [28]. Then, we obtain the final momentum distribution by averaging the momentum over the focal volume of the pulses (see Sec. II). Finally, the release times are determined with the procedure sketched in Fig. 7. The result is shown in Fig. 9. Clearly, it also agrees excellently with experimental data. Thus, it indicates that the deviation of the release time of the second electron between the experimental data and the prediction of the tunneling theory is not from the above approximations of the tunneling theory. The second electron really escapes earlier than the prediction of the independent-tunneling theory.

In our model the Heisenberg-core potential was introduced to reproduce the first and the second ionization potentials of the target, which is an essential condition for accurate description of SDI. We would like to state that our results are structurally stable and do not depend on the choice of parameter α. When α is changed, the value of ξ should be changed correspondingly to keep the second ionization potential of the model atom stable. Otherwise, if one changes the value of α while keeping ξ unchanged, the ionization potentials of the model atom shift significantly, as shown in Figs. 10(a) and 10(b). It can be predictable that the shift of ionization potentials of the model atom will influence the ionization times of both electrons significantly. This does not mean that our model is not stable. As addressed in Sec. II, the necessary condition for a model to accurately describe SDI is that the model should reproduce the ionization potentials of the investigated target and keep the ionization potentials stable when changing the corresponding parameters. Thus, in the Heisenberg-core potential classical model, the value of ξ should be changed correspondingly as α changes to keep the ionization potential unchanged. In Fig. 10(c) we show the corresponding value of ξ for different values of α, which keeps the second ionization potential (-1.065 a.u.) of the model atom unchanged. Under this condition, we calculated the time delay between the two ionization steps in SDI with the HPCM. The results are shown in Fig. 10(d). Definitely, these results are stable upon α. Note that the computational time increases significantly as α increases because of the increasing stiffness of the Heisenberg-core potential.

We remark that the success of the classical treatment is not a result of this particular potential. Recently, Wang *et al.* [41] have shown that the experimental results can also be quantitatively reproduced by a soft-core potential classical model when the first and the second ionization potentials are artificially adjusted to the investigated target at each ionization step. This makes it easy to accept that our results are stable and do not depend on the parameters α and ξ of the Heisenberg-core potential.

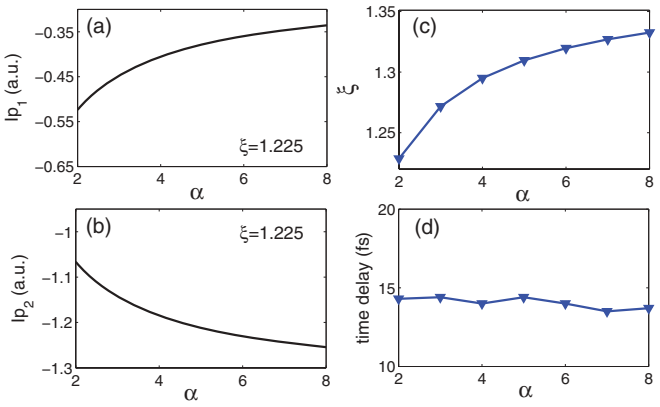

FIG. 10. (Color online) (a) and (b) The first and the second ionization potentials of the model atom as a function of α for $\xi = 1.225$. (c) The value of ξ that keeps the second ionization potential (-1.065 a.u.) unchanged for changing α. (d) The mean value of the time delay between the two ionization steps in SDI for different values of α, where the corresponding value of ξ is from (c). The laser intensity is 4.0 PW/cm^2 and the pulse duration is 33 fs. Here the volume effect is not taken into account.

In the work of Wang *et al.*, the electron correlation is not taken into account. The excellent agreement between their calculations and the experimental data leads us to suspect that the deviation between the prediction of the tunneling theory and the experimental data is attributed to the inaccuracy of the empirical formula for the ionization rate [42]. In the ionization rate formula [42], the ionization rate does not depend on the sign of the magnetic quantum number. However, recently Barth *et al.* theoretically predicted the dependence of the ionization rate on the sign of the magnetic quantum number [43]. This prediction was experimentally confirmed by Herath *et al.* [44]. These facts give us sufficient reasons to reexamine the accuracy of the tunneling formula.

IV. SUMMARY

In conclusion, we have numerically investigated SDI of Ar by the elliptical pulses. It would be expected that only a fully quantum model could quantitatively reproduce the SDI experimental results. In this work, we demonstrated that a simple classical model reproduced all of the experimental observations at the quantitative level. Thus, it provides a simple way to investigate the complex multielectron dynamics in strong-field processes where the fully quantum approach is a great challenge. Recently, with this correlated classical model, we examined the multielectron effect in strong-field SDI and predicted that electron correlations in SDI left imprints on the angular distribution of the first electron [45]. Undoubtedly, our work will inspire further investigations on the multielectron dynamics in strong-field double and multiple ionizations.

ACKNOWLEDGMENTS

We thank Dr. Pfeiffer for providing us with his experimental data. This work was supported by the National Science Fund (No. 60925021 and No. 11234004) and the 973 Program of China (No. 2011CB808103).

[1] P. B. Corkum, Phys. Rev. Lett. **71**, 1994 (1993); K. C. Kulander, J. Cooper, and K. J. Schafer, Phys. Rev. A **51**, 561 (1995).
[2] D. N. Fittinghoff, P. R. Bolton, B. Chang, and K. C. Kulander, Phys. Rev. Lett. **69**, 2642 (1992); B. Walker, B. Sheehy, L. F. DiMauro, P. Agostini, K. J. Schafer, and K. C. Kulander, *ibid.* **73**, 1227 (1994); J. B. Watson, A. Sanpera, D. G. Lappas, P. L. Knight, and K. Burnett, *ibid.* **78**, 1884 (1997); S. Larochelle, A. Talebpour, and S. L. Chin, J. Phys. B **31**, 1201 (1998).
[3] Th. Weber *et al.*, Nature (London) **405**, 658 (2000).
[4] R. Lafon, J. L. Chaloupka, B. Sheehy, P. M. Paul, P. Agostini, K. C. Kulander, and L. F. DiMauro, Phys. Rev. Lett. **86**, 2762 (2001).
[5] E. Eremina *et al.*, J. Phys. B **36**, 3269 (2003).
[6] J. L. Chaloupka, J. Rudati, R. Lafon, P. Agostini, K. C. Kulander, and L. F. DiMauro, Phys. Rev. Lett. **90**, 033002 (2003).
[7] C. Guo and G. N. Gibson, Phys. Rev. A **63**, 040701 (2001).
[8] Th. Weber *et al.*, Phys. Rev. Lett. **84**, 443 (2000); R. Moshammer *et al.*, *ibid.* **84**, 447 (2000); B. Feuerstein *et al.*, *ibid.* **87**, 043003 (2001).
[9] A. Rudenko, K. Zrost, B. Feuerstein, V. L. B. de Jesus, C. D. Schröter, R. Moshammer, and J. Ullrich, Phys. Rev. Lett. **93**, 253001 (2004).
[10] M. Weckenbrock, A. Becker, A. Staudte, S. Kammer, M. Smolarski, V. R. Bhardwaj, D. M. Rayner, D. M. Villeneuve, P. B. Corkum, and R. Dörner, Phys. Rev. Lett. **91**, 123004 (2003); **92**, 213002 (2004).
[11] R. Moshammer *et al.*, J. Phys. B **36**, L113 (2003).
[12] A. Staudte *et al.*, Phys. Rev. Lett. **99**, 263002 (2007); A. Rudenko, V. L. B. de Jesus, Th. Ergler, K. Zrost, B. Feuerstein, C. D. Schröter, R. Moshammer, and J. Ullrich, *ibid.* **99**, 263003 (2007).
[13] T. Brabec, M. Y. Ivanov, and P. B. Corkum, Phys. Rev. A **54**, R2551 (1996).
[14] U. Eichmann, M. Dörr, M. Maeda, W. Becker, and W. Sandner, Phys. Rev. Lett. **84**, 3550 (2000).
[15] J. S. Parker, B. J. S. Doherty, K. T. Taylor, K. D. Schultz, C. I. Blaga, and L. F. DiMauro, Phys. Rev. Lett. **96**, 133001 (2006).
[16] A. Becker and F. H. M. Faisal, Phys. Rev. Lett. **84**, 3546 (2000); R. Kopold, W. Becker, H. Rottke, and W. Sandner, *ibid.* **85**, 3781 (2000); C. F. Faria, X. Liu, A. Sanpera, and M. Lewenstein, Phys. Rev. A **70**, 043406 (2004); S. P. Goreslavski and S. V. Popruzhenko, Opt. Express **8**, 395 (2001).
[17] M. Lein, E. K. U. Gross, and V. Engel, Phys. Rev. Lett. **85**, 4707 (2000); J. S. Prauzner-Bechcicki, K. Sacha, B. Eckhardt, and J. Zakrzewski, *ibid.* **98**, 203002 (2007); C. Ruiz, L. Plaja, L. Roso, and A. Becker, *ibid.* **96**, 053001 (2006); Q. Liao and P. Lu, Phys. Rev. A **82**, 021403(R) (2010); Q. Liao, Y. Zhou, C. Huang, and P. Lu, New J. Phys. **14**, 013001 (2012).
[18] K. Sacha and B. Eckhardt, Phys. Rev. A **63**, 043414 (2001).

[19] R. Panfili, S. L. Haan, and J. H. Eberly, Phys. Rev. Lett. **89**, 113001 (2002); P. J. Ho, R. Panfili, S. L. Haan, and J. H. Eberly, *ibid.* **94**, 093002 (2005); S. L. Haan, L. Breen, A. Karim, and J. H. Eberly, *ibid*. **97**, 103008 (2006); F. Mauger, C. Chandre, and T. Uzer, *ibid.* **102**, 173002 (2009); F. Mauger, A. Kamor, C. Chandre, and T. Uzer, *ibid.* **108**, 063001 (2012).

[20] Y. Zhou, Q. Liao, and P. Lu, Phys. Rev. A **80**, 023412 (2009); **82**, 053402 (2010); Y. Zhou, C. Huang, and P. Lu, *ibid.* **84**, 023405 (2011); Y. Zhou *et al.*, Opt. Lett. **36**, 2758 (2011); A. Tong *et al.*, Opt. Express **18**, 9064 (2010); C. Huang *et al.*, *ibid*. **19**, 5627 (2011); Y. Zhou *et al.*, Chin. Phys. Lett. **25**, 3950 (2008); **27**, 123201 (2010).

[21] B. Chang, P. R. Bolton, and D. N. Fittinghoff, Phys. Rev. A **47**, 4193 (1993).

[22] K. I. Dimitriou, S. Yoshida, J. Burgdörfer, H. Shimada, H. Oyama, and Y. Yamazaki, Phys. Rev. A **75**, 013418 (2007).

[23] N. I. Shvetsov-Shilovski, A. M. Sayler, T. Rathje, and G. G. Paulus, Phys. Rev. A **83**, 033401 (2011).

[24] P. Dietrich, N. H. Burnett, M. Ivanov, and P. B. Corkum, Phys. Rev. A **50**, R3585 (1994).

[25] D. N. Fittinghoff, P. R. Bolton, B. Chang, and K. C. Kulander, Phys. Rev. A **49**, 2174 (1994).

[26] C. M. Maharjan, A. S. Alnaser, X. M. Tong, B. Ulrich, P. Ranitovic, S. Ghimire, Z. Chang, I. V. Litvinyuk, and C. L. Cocke, Phys. Rev. A **72**, 041403(R) (2005).

[27] X. Wang and J. H. Eberly, Phys. Rev. A **86**, 013421 (2012).

[28] A. N. Pfeiffer *et al.*, Nat. Phys. **7**, 428 (2011).

[29] A. N. Pfeiffer *et al.*, New J. Phys. **13**, 093008 (2011).

[30] A. Fleischer, H. J. Wörner, L. Arissian, L. R. Liu, M. Meckel, A. Rippert, R. Dörner, D. M. Villeneuve, P. B. Corkum, and A. Staudte, Phys. Rev. Lett. **107**, 113003 (2011).

[31] Y. Zhou *et al.*, Opt. Express **18**, 632 (2010); **18**, 16025 (2010); **19**, 2301 (2011).

[32] X. Wang and J. H. Eberly, Phys. Rev. Lett. **103**, 103007 (2009).

[33] X. Wang and J. H. Eberly, arXiv:1102.0221v1.

[34] Y. Zhou, C. Huang, Q. Liao, and P. Lu, Phys. Rev. Lett. **109**, 053004 (2012).

[35] D. Bauer, Phys. Rev. A **56**, 3028 (1997).

[36] C. L. Kirschbaum and L. Wilets, Phys. Rev. A **21**, 834 (1980).

[37] D. Zajfman and D. Maor, Phys. Rev. Lett. **56**, 320 (1986).

[38] J. S. Cohen, Phys. Rev. A **54**, 573 (1996); **56**, 3583 (1997); W. A. Beck, L. Wilets, and M. A. Alberg, *ibid.* **74**, 052706 (2006)

[39] P. B. Lerner, K. J. LaGattuta, and J. S. Cohen, Phys. Rev. A **49**, R12 (1994); D. A. Wasson and S. E. Koonin, *ibid*. **39**, 5676 (1989); E. Lötstedt, T. Kato, and K. Yamanouchi, Phys. Rev. Lett. **106**, 203001 (2011); C. Huang *et al.*, Opt. Express **20**, 11700 (2012).

[40] P. Wang *et al.*, Opt. Lett. **30**, 664 (2005).

[41] X. Wang, J. Tian, A. N. Pfeiffer, C. Cirelli, U. Keller, and J. H. Eberly, arXiv:1208.1516v1.

[42] X. M. Tong and C. D. Lin, J. Phys. B **38**, 2593 (2005).

[43] I. Barth and O. Smirnova, Phys. Rev. A **84**, 063415 (2011).

[44] T. Herath, L. Yan, S. K. Lee, and W. Li, Phys. Rev. Lett. **109**, 043004 (2012).

[45] Y. Zhou, C. Huang, and P. Lu, Opt. Express **20**, 20201 (2012).